Journal of Solid State Electrochemistry (2019) 23:1911–1927
https://doi.org/10.1007/s10008-019-04260-2

ORIGINAL PAPER

# Electrochemical performance of carbon paper supercapacitor using sodium molybdate gel polymer electrolyte and nickel molybdate electrode

Yibing Xie[1] · Yanchen Zhang[1]

Received: 12 February 2019 / Revised: 18 March 2019 / Accepted: 24 March 2019 / Published online: 15 May 2019


## Abstract

Graphene oxide–modified poly (vinyl alcohol)/sodium sulfate-sodium molybdate (GO/PVA-$Na_2SO_4$-$Na_2MoO_4$, GPSS) gel polymer electrolyte and nickel molybdate ($NiMoO_4$) electrode are integrated to fabricate carbon paper (CP) supercapacitor to improve capacitance performance. GO in PVA gel can introduce an effective ion transport pathway to improve ionic conductivity of gel polymer electrolyte. The ionic conductivity increases from 3.73 mS $cm^{-1}$ for PVA-$Na_2SO_4$ to 6.46 mS $cm^{-1}$ for GO/PVA-$Na_2SO_4$ at optimal GO mass ratio of 0.6% in GO/PVA gel. It also obviously increases from 4.33 mS $cm^{-1}$ for PVA-$Na_2SO_4$-$Na_2MoO_4$ to 28.86 mS $cm^{-1}$ for GO/PVA-$Na_2SO_4$-$Na_2MoO_4$. Both $Na_2MoO_4$ electrolyte and $NiMoO_4$ electrode show reversible redox electroactivity to provide superior pseudocapacitance. Accordingly, the CP supercapacitor using GPSS gel shows specific capacitance of 41.67 mF $cm^{-2}$ and energy density of 70.02 mWh $m^{-2}$ at 0.5 mA $cm^{-2}$, presenting higher performance than 15.91 mF $cm^{-2}$ and 26.74 mWh $m^{-2}$ using GO/PVA-$Na_2SO_4$ gel. Furthermore, the $NiMoO_4$/CP supercapacitor using GPSS gel shows even higher specific capacitance of 78.18 mF $cm^{-2}$ and energy density of 131.39 mWh $m^{-2}$ at 0.5 mA $cm^{-2}$. It also exhibits high cycling capacitance retention of 85% at 0.5 mA $cm^{-2}$ for 1000 cycles. The improved capacitance performance of CP supercapacitor using $Na_2MoO_4$ gel polymer electrolyte and $NiMoO_4$ electrode is ascribed to reversible redox reaction of Mo(VI)/Mo(V), Mo(VI)/Mo(IV), and Ni(II)/Ni(III). The $NiMoO_4$/CP supercapacitor using GO/$Na_2MoO_4$ gel polymer electrolyte becomes desirable for the promising application in energy storage devices.

**Keywords** Gel polymer electrolyte · Graphene oxide · Sodium molybdate electrolyte · Nickel molybdate electrode · Carbon paper supercapacitor

## Introduction

Supercapacitors, consisting of electric double layer capacitors (EDLCs) and pseudo-capacitors, become feasible energy storage devices due to high power density and long cycling life [1, 2]. The electrochemical performance of supercapacitors mainly depends on the properties of electrode and electrolyte [3, 4]. EDLC achieves the energy storage through ion adsorption and desorption at electrode/electrolyte interface to form an electric double layer. The accumulation of electrons at the electrode is a non-Faradaic process. Comparatively, pseudo-capacitors achieve the energy storage through the rapid and reversible redox reaction at electrode/electrolyte interface. The accumulation of electrons at the electrode is a Faradaic process where the electrons produced by the redox reaction are transferred across the electrolyte/electrode interface. The pseudo-capacitors could exhibit higher capacitance performance than EDLCs [5–7]. Transition metal oxides have been widely investigated because of the high theoretical capacity and cycling stability [8–12]. The polyoxometalates such as $NiMoO_4$, $NiCo_2O_4$, and $CoMoO_4$ exhibit high theoretical capacity, which is attributed to the multiple Faradic redox reaction [13–16]. Electrolyte also plays an important role in the electrochemical performance of the supercapacitors [17, 18]. However, traditional liquid electrolytes show some obvious drawbacks such as leakage, corrosion, and even explosion [19]. The solid electrolytes show low ionic conductivity

✉ Yibing Xie
ybxie@seu.edu.cn

[1] School of Chemistry and Chemical Engineering, Southeast University, Nanjing 211189, China

[20]. To well combine both the advantages of the liquid electrolyte and solid electrolyte, the gel polymer electrolyte (GPE) has attracted much attention, such as PVA-$H_3PO_4$ [21], PVA-$H_2SO_4$ [22], PVA-KOH [23], PVA/PVC-$Na_2SO_4$ [24], PEO-KOH-$H_2O$ [25], and PAA-KCl [26]. The redox additives or mediators in electrolytes can carry out the redox reaction to provide pseudocapacitance [27]. The inorganic additives include KI [28], $K_3[Fe(CN)_6]$ [29], $Na_2MoO_4$ [30–32], $VOSO_4$ [33], etc. The organic additives include P–benzenediol [34], P-phenylenediamine [29], indigo carmine [35], 2-mercaptopyridine [36], and alizarin red S [37]. $Na_2MoO_4$ has been widely used as redox additives of electrolyte to improve the electrochemical performance. Graphene oxide (GO) keeps large specific surface area and abundant oxygen-containing functional groups and can disperse well in polar solvents. It becomes a useful additive to improve the ionic conductivity and electrochemical performance of the supercapacitors and other devices. Graphene oxide sheet is able to form high-speed channel in the gel polymer electrolytes and shorten ion transfer pathway, thus improving the ionic conductivity of gel polymer electrolytes [38, 39].

In this study, the redox $Na_2MoO_4$ as redox electrolyte and $NiMoO_4$ as redox electrode are applied to construct carbon paper (CP) solid-state supercapacitor to improve overall capacitance performance. GO/PVA-$Na_2SO_4$-$Na_2MoO_4$ (GPSS) gel polymer is used as the working electrolyte to improve ionic conductivity and meanwhile provide pseudocapacitance. $NiMoO_4$ supported on CP ($NiMoO_4$/CP) used the working electrode to provide pseudocapacitance. Accordingly, GPSS//$NiMoO_4$/CP solid-state supercapacitor by introducing the redox electrolyte and redox electrode is expected to have superior capacitance performance for electrochemical energy storage application.

## Experimental section

### Materials

Polyvinyl alcohol (PVA) and sodium sulfate anhydrous ($Na_2SO_4$, analytical reagent, purity > 99%) were purchased from Chengdu Kelong chemical reagent factor. Sodium molybdate dehydrate ($Na_2MoO_4{\cdot}2H_2O$, analytical reagent, purity > 99%), nickel nitrate ($Ni(NO_3)_2{\cdot}6H_2O$, analytical reagent, purity > 98%), potassium permanganate ($KMnO_4$, analytical reagent, purity > 99.5%), sulfuric acid ($H_2SO_4$, analytical reagent, purity > 98%), hydrogen peroxide ($H_2O_2$, analytical reagent, purity = 30%), sodium nitrate ($NaNO_3$, analytical reagent, purity > 99%), nickel molybdate, ammonium persulfate ($(NH_4)_2S_2O_8$, analytical reagent, purity > 98%) were purchased from Sinopharm chemical reagent Co., Ltd. Deionized water was used throughout all experiments.

### Preparation of gel polymer electrolyte

Graphene oxide (GO) was prepared by the modified Hummer method. Briefly, 1.5 g graphite powder was combined with 5 g $NaNO_3$ in a 1000-mL breaker. Seventy-five milliliters $H_2SO_4$ was mixed under continuously stirring for 15 min at room temperature. After the breaker is migrated into an ice-water bath, 9 g $KMnO_4$ was dissolved into the mixture solution under vigorous stirring for 30 min. The reaction was continued at room temperature for 48 h on the basis of removing the ice-water bath. Then, 138 mL deionized water was transferred into the precursor and kept the stirring for 10 min to obtain brown suspension. Afterwards, 30 mL 0.3 M $H_2O_2$ and 420 mL hot deionized water were poured into the breaker gradually. This suspension was centrifugalized and the product was washed with 0.6 M $H_2SO_4$ and 0.3 M $H_2O_2$ solution and deionized water for several times. Finally, the sample was dried at 60 °C for 8 h in a hot air oven. Figure 1a shows the formation process of gel polymer electrolyte. GO/PVA-$Na_2SO_4$-$Na_2MoO_4$ (GPSS) gel polymer electrolyte was fabricated through a solution-mixing method. Firstly, 0.5 g PVA was dissolved in 5 mL deionized water which contained different amounts of GO (0.2, 0.4, 0.6, 0.8, 1.0 mg $mL^{-1}$) at 80 °C for 1 h to form homogeneous mixtures under continuously stirring. One milliliter 0.5 M $Na_2SO_4$ and 5 mL 0.08 M $Na_2MoO_4{\cdot}2H_2O$ were added into the mixtures. Finally, the solution was cooled down at room temperature to obtain gel polymer electrolyte. The gel polymer electrolyte with different GO mass ratios was denoted as GPSS1, GPSS2, GPSS3, GPSS4, GPSS5, and GPSS6, respectively. For a comparison, PVA-$Na_2SO_4$ (PS), GO/PVA-$Na_2SO_4$ (GPS), and PVA-$Na_2SO_4$-$Na_2MoO_4$ (PSS) gel polymer electrolytes were prepared using the same process.

### Preparation of $NiMoO_4$/CP electrode

The carbon paper (CP, 5 × 1 × 0.05 cm) and $NiMoO_4$/CP electrodes were prepared as follows. Figure 1b shows the preparation process of CP electrode and $NiMoO_4$/CP electrode. The pristine CP conducted the activation treatment. CP was washed with anhydrous ethanol and deionized water. CP and the mixture solution of 24 mL 3 M $H_2SO_4$ and 12 mL 8.8 M $H_2O_2$ were transferred into a Teflon-lined stainless steel autoclave. The hydrothermal reaction was conducted at 180 °C for 12 h. Afterwards, two pieces of CP were immersed parallelly into an electrochemical cell containing 50 mL 17.5 mM $(NH_4)_2S_2O_8$ solution and performed by the Multi-Potential Steps program of the electrochemical workstation (CHI760C, CH Instruments) at an anodization voltage of 10 V for 5 min in a two-electrode system. The obtained sample was the activated CP electrode. Concerning $NiMoO_4$/CP electrode, 0.25 mmol $Ni(NO_3)_2{\cdot}6H_2O$, 0.25 mmol $Na_2MoO_4{\cdot}2H_2O$, and 0.5 mmol urea were dissolved in deionized water

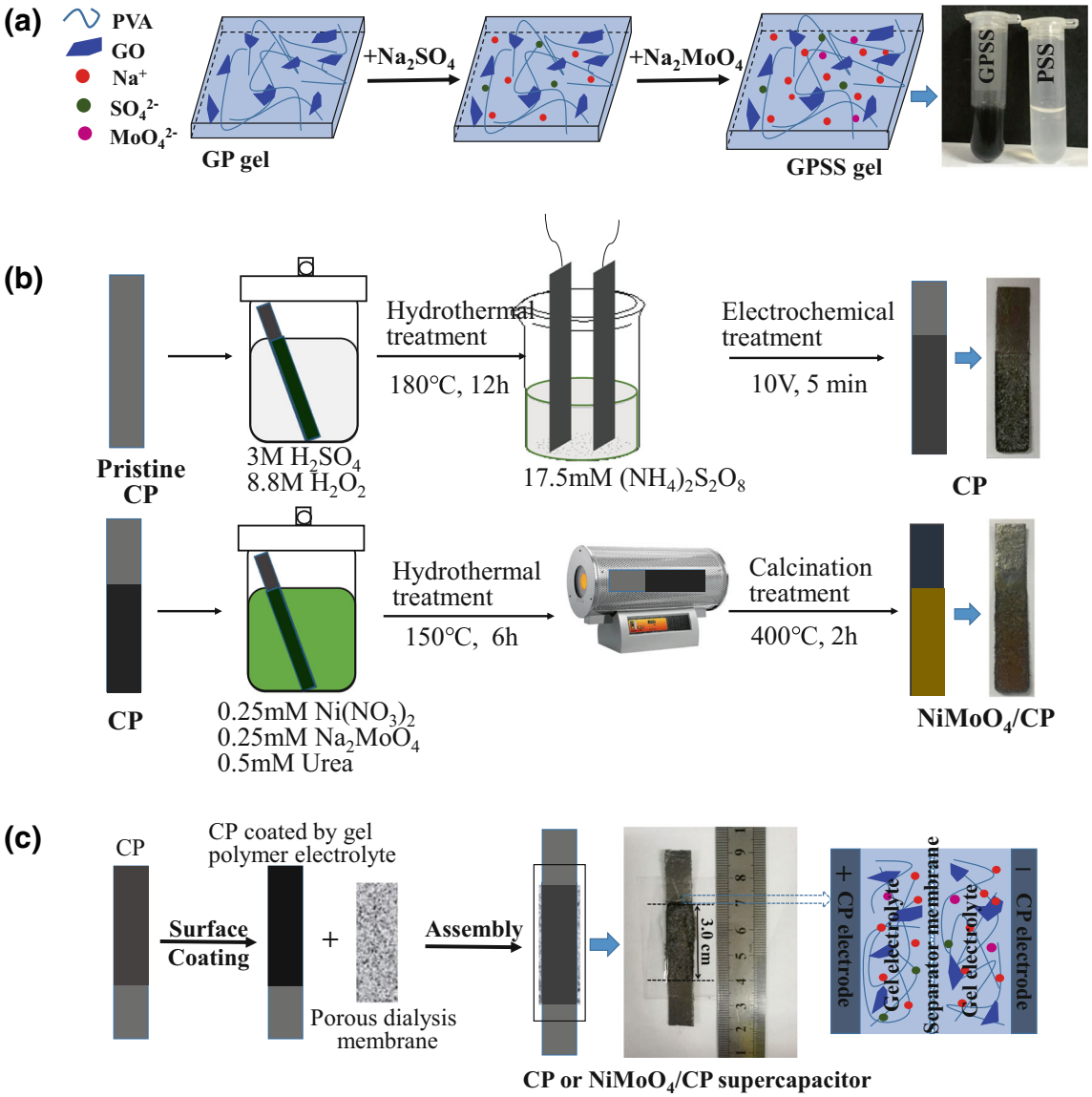


**Fig. 1** Schematics and photographs illustrating the formation process of GO/PVA-$Na_2SO_4$-$Na_2MoO_4$ (GPSS) gel polymer electrolyte (**a**), preparation process of CP and $NiMoO_4$/CP electrode (**b**), and assembly process of GO/PVA-$Na_2SO_4$-$Na_2MoO_4$ gel-involved CP or $NiMoO_4$/CP supercapacitor (**c**)

under constant magnetic stirring and were transferred into Teflon-lined stainless steel autoclave liners. The CP sheet was putted into the above solution to conduct the hydrothermal reaction at 150 °C for 6 h. Finally, the as-prepared product was calcinated at 400 °C for 1 h in pure argon to obtain $NiMoO_4$/CP electrode. The loading amount of $NiMoO_4$ is 10 mg on the surface of CP substrate.

## Construction of supercapacitor

Figure 1c shows the assembly process of CP or $NiMoO_4$/CP supercapacitor. The CP or $NiMoO_4$/CP electrodes were covered with gel polymer electrolyte through spin-coating and air-drying processes at room temperature to evaporate excessive water. Two symmetric electrodes were stacked together by using porous dialysis membrane as the separator and wrapped with ultra-thin plastic film to form solid-state supercapacitors. Concerning GPSS electrolyte, GO sheet contributes to building up the rapid ion transport pathway for electrolyte ions. $Na_2MoO_4$ with redox activity can provide Faradic capacitance. $Na_2SO_4$ can provide free transport ions as supporting electrolyte. So, the GPSS//CP or GPSS//$NiMoO_4$/CP supercapacitor is designed to have dramatically improved electrochemical performance.

## Characterization and measurement

The surface morphology and microstructure of the carbon paper electrode were characterized by using a scanning electron microscope (SEM, Zeiss Ultra Plus) at an accelerating voltage of 3 kV. Energy dispersive X-ray (EDX, Oxford

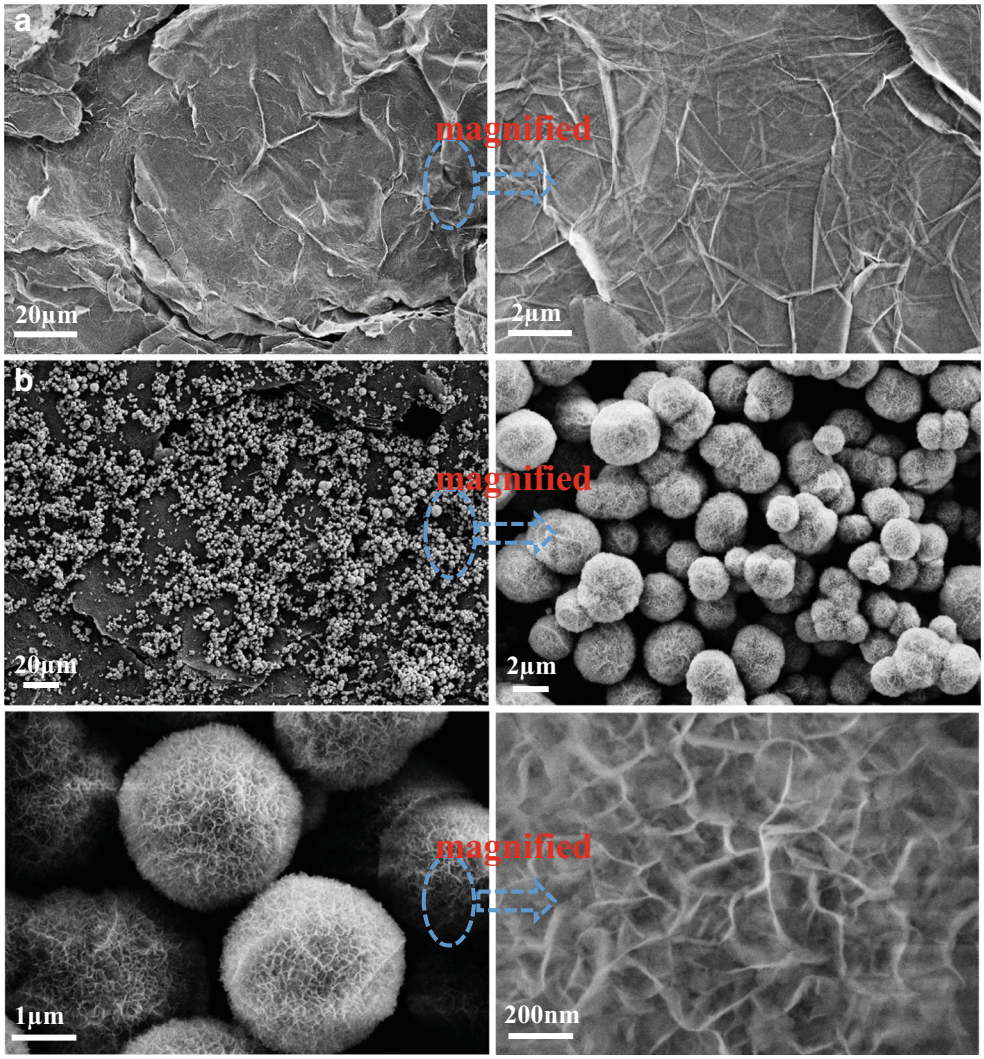


**Fig. 2** SEM images of the synthesized CP (**a**) and $NiMoO_4$/CP (**b**)

ISIS 310) spectroscopy was conducted to identify the element components of GPSS. Raman spectroscopy was measured on a Raman spectrometer (Raman, Oceanoptics Benchtop Raman System) using a He-Ne laser emitting at 785 nm excitation in the wave number range of 0–2500 $cm^{-1}$. All the electrochemical studies were carried out at room temperature

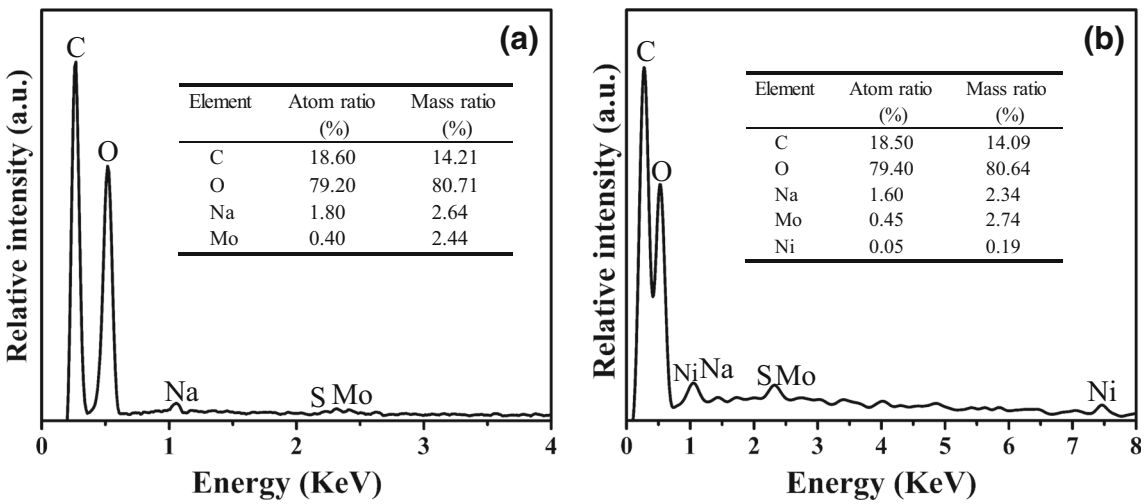


**Fig. 3** EDX spectra of GPSS-coated CP electrode and GPSS-coated $NiMoO_4$/CP electrode

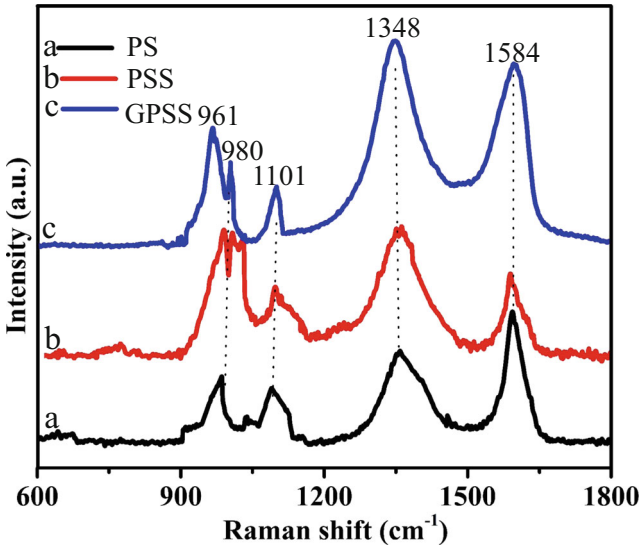


**Fig. 4** Raman spectra of PS (**a**), PSS (**b**), and GPSS (**c**)

using CHI760 electrochemical workstation. Cyclic voltammetry (CV) and galvanostatic charge–discharge (GCD) measurement were performed at a potential range from 0 to 1.1 V, scan rates from 5 to 100 mV $s^{-1}$ for CV, and current density from 0.5 to 4.0 mA $cm^{-2}$ for GCD. Electrochemical impedance spectroscopy (EIS) was investigated from 0.01–100 Hz with an electrode potential of 0 V and a potential amplitude of 5 mV. In addition, the areal specific capacitance ($C_s$, mF $cm^{-2}$), energy density ($E$, mWh $m^{-2}$), and power density ($P$, mW $cm^{-2}$) are calculated by using the following equations (Eqs. (1–4)).

$$C_s = \frac{1}{2s \times \Delta V}\int_{V_0}^{V_0+\Delta V} i dV. \quad (1)$$

$$C_s = \frac{Q}{\Delta V \times S} = \frac{I \times t}{\Delta V \times S} \quad (2)$$

$$E = \frac{I \times t \times \Delta V}{2S} \times \frac{10000}{3600} = \frac{10000}{2 \times 3600} C_s \Delta V^2 \quad (3)$$

$$P = \frac{I \times \Delta V}{2S} \quad (4)$$

where $C_s$ is the areal specific capacitance, $s$ is the scan rate (V $s^{-1}$), $\Delta V$ is the voltage between the upper and lower potential limit (V), $i$ is the current density (A $cm^{-2}$), $I$ is the charge–discharge current, $t$ is the time of discharge, and $S$ is the contact area of two electrodes. The equivalent series resistance ($ESR$) and the effective diffusion coefficient ($D$) are calculated from the following equations (Eqs. (5–6)).

$$ESR = \frac{IR_{\text{drop}}}{2I} \quad (5)$$

$$D = \frac{L^2}{W_T} \quad (6)$$

where $IR_{\text{drop}}$ is the Ohmic voltage drop in each discharge curve, $I$ is the applied discharge current, $L$ is the effective diffusion distance, and $W_T$ is the diffusion time constant. The ionic conductivity ($\sigma$) of gel polymer electrolyte can be determined by EIS test through the following equation.

$$\sigma = \frac{L}{R_b \times S} \quad (7)$$

where $L$ (cm) is the distance between the two pieces of carbon paper, $R_b$ (ohm) is the bulk resistance, and $S$ ($cm^2$) is the contact area of the electrolyte with the two pieces of carbon paper.

## Results and discussion

### Morphological characterization

Figure 2 shows SEM images of CP and $NiMoO_4$/CP. The surface of CP becomes rough and crumpled after the activation treatment. The overlap between the graphite layers becomes wider and the sheet-like structure is formed. In view of the high-magnification SEM image, the edge of the graphite layers is curled slightly. The graphite layers appear the broken boundary, which leads to forming graphite fragments with different shapes. The gaps between these fragments provide the more feasible interface for electrolyte ion transport. Concerning $NiMoO_4$/CP, the spherical particles of $NiMoO_4$ are grown uniformly on the surface of CP. The particles have an average diameter of 2 μm. The spherical $NiMoO_4$ provides high specific surface area and reactive sites, accordingly enhancing the electrochemical performance.

Figure 3 shows the EDX spectrum of GPSS gel polymer electrolyte coated on CP and $NiMoO_4$/CP electrodes. The atomic ratio and weight ratio of different elements are displayed in the inset of Fig. 4. Two obvious energy dispersive peaks at 0.26 and 0.52 keV are ascribed to carbon and oxygen element, respectively. The atom ratio of oxygen element is as high as 79.20% because PVA, $NaSO_4$, $Na_2MoO_4$, and GO all contain oxygen element. The energy dispersive peak at 2.23 keV is ascribed to the sulfate element of $NaSO_4$. Its very low content can be neglected. Comparatively, two energy dispersive peaks at 0.75 and 7.45 keV are ascribed to nickel element of $NiMoO_4$. The atom ratio of molybdenum element in GPSS-coated $NiMoO_4$/CP is higher than that in GPSS-coated CP. It proves the growth of $NiMoO_4$ on the surface of CP substrate. The mole ratio of $NiMoO_4$ vs. $Na_2MoO_4$ is1:8.

Figure 4 shows the Raman spectra of PS, PSS, and GPSS coated on CP. All samples show four obvious characteristic peaks at around 980 $cm^{-1}$, 1101 $cm^{-1}$, 1348 $cm^{-1}$, and 1584 $cm^{-1}$. The peaks at 980 $cm^{-1}$ and 1101 $cm^{-1}$ are assigned

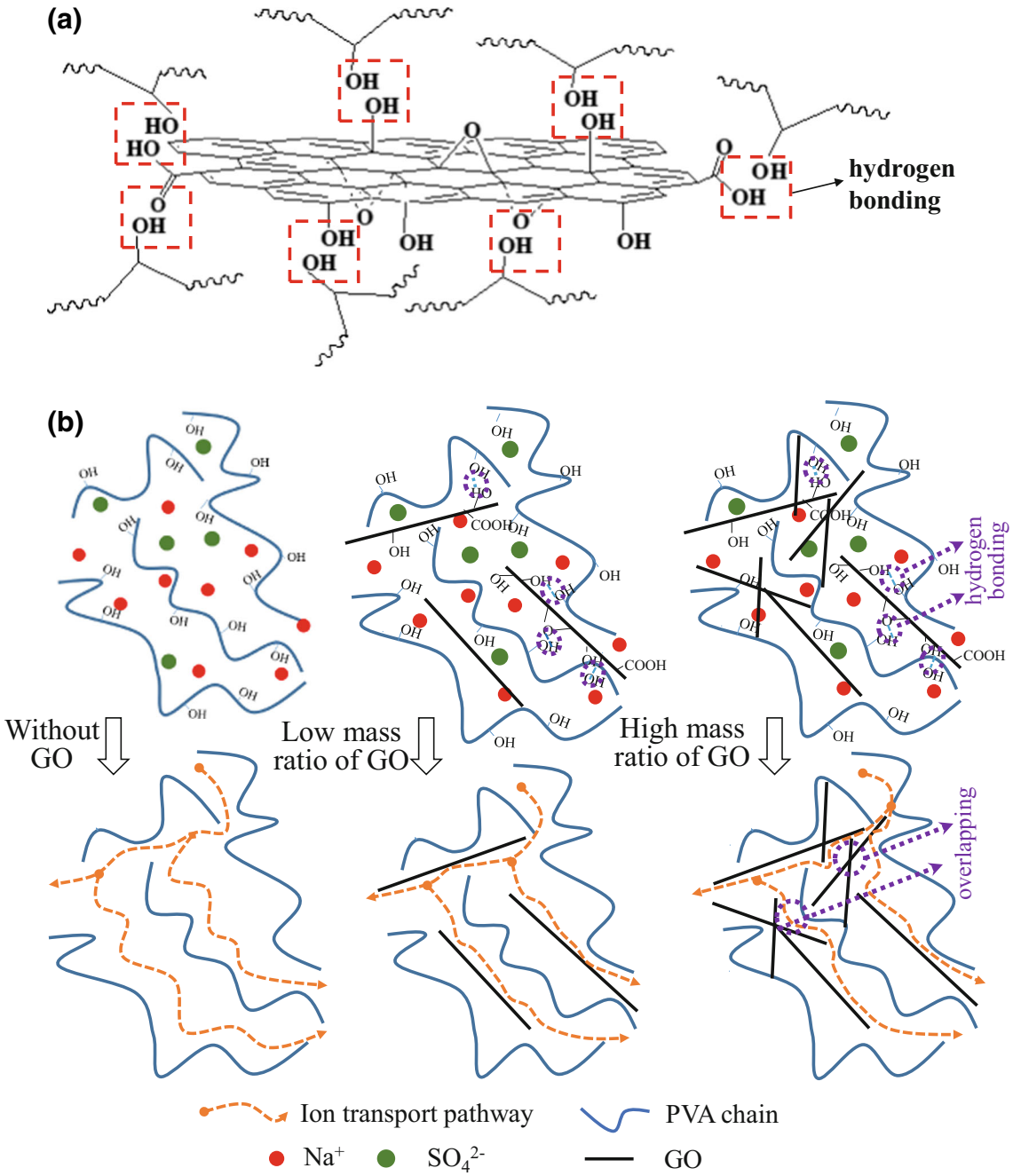


**Fig. 5** Schematic illustrating the hydrogen-bonding interaction between GO and PVA (**a**), ion transport mechanism in PVA-$Na_2SO_4$ gel polymer electrolyte without GO (**b**), low mass ratio of GO, and high mass ratio of GO.

to the symmetric stretching vibration and deformation vibration of S–O bond in sulfate. The peak at 1348 $cm^{-1}$ corresponds to the D band, which is associated with the $A_{1g}$ vibration mode, the $sp^3$ hybridization carbon atom with disordered graphite structure. The peak at 1584 $cm^{-1}$ corresponds to the G band, which is associated with the $E_{2g}$ vibrational mode of $sp^2$ hybridization carbon atom with crystal graphite structure [40]. The peak at 961 $cm^{-1}$ shown in curve b and c is ascribed to symmetric stretching vibration of Mo=O bond in molybdate [41]. Comparatively, GPSS shows higher peak intensity at 1348 $cm^{-1}$ and 1584 $cm^{-1}$ than PSS, which results from the D band and G band of GO. The $I_D/I_G$ ratio of PS, PSS, and GPSS is 0.70, 1.59, and 1.13, respectively. In general, the $I_D/I_G$ ratios are related to crystalline, defect, and functional group of graphite [42]. PSS and GPSS exhibit high ratio of $I_D/I_G$ than PS. It is attributed to the extra defects caused by the interaction between $NaMoO_4$ and graphite [43]. The carbon defects favor the adsorption and growth of $NaMoO_4$ on activated graphite carbon paper, providing additional active sites for the charge storage [44]. Furthermore, GPSS exhibits lower $I_D/I_G$ ratio than

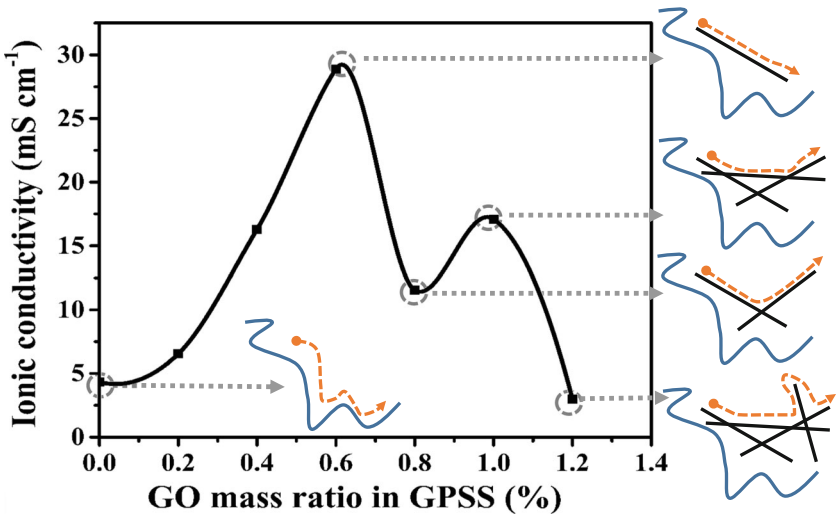


**Fig. 6** Ionic conductivity and effective ion transport pathway of GPSS gel polymer electrolyte with different mass ratios of GO

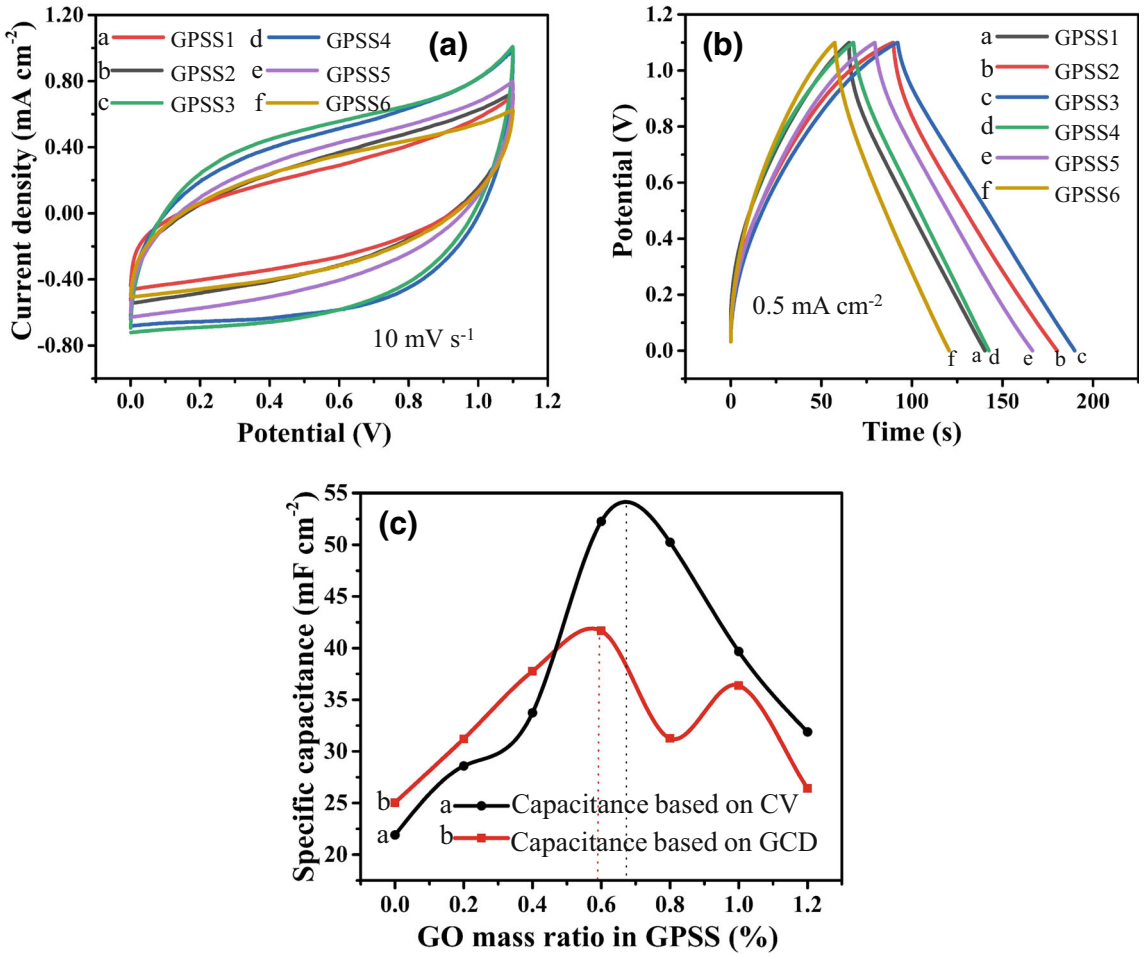


**Fig. 7** **a** CV curves at a scan rate of 10 mV $s^{-1}$; **b** GCD curves at 0.5 mA $cm^{-2}$; **c** Specific capacitance of GPSS//CP supercapacitor with different GO mass ratios

PSS. Herein, partially oxidized GO presents lower $I_D/I_G$ ratio than fully activated graphite carbon paper. Accordingly, the introduction of GO could decrease overall $I_D/I_G$ ratio of gel polymer–modified activated graphite carbon paper electrode.

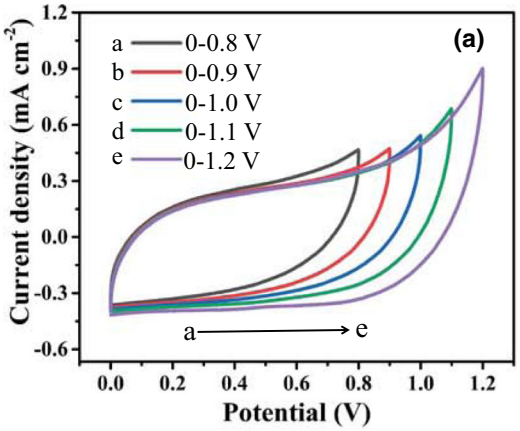
(a)
a 0-0.8 V
b 0-0.9 V
c 0-1.0 V
d 0-1.1 V
e 0-1.2 V
a → e
Current density (mA cm-2)
Potential (V)

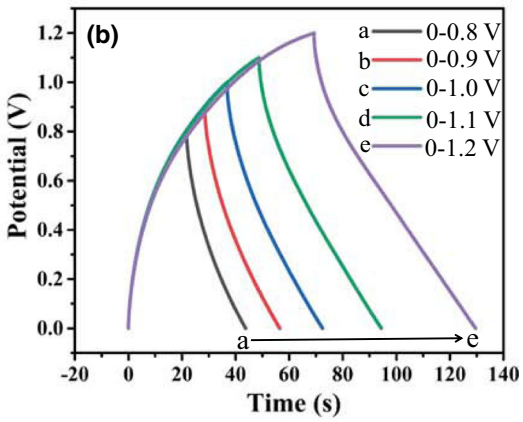
(b)
a 0-0.8 V
b 0-0.9 V
c 0-1.0 V
d 0-1.1 V
e 0-1.2 V
a → e
Potential (V)
Time (s)

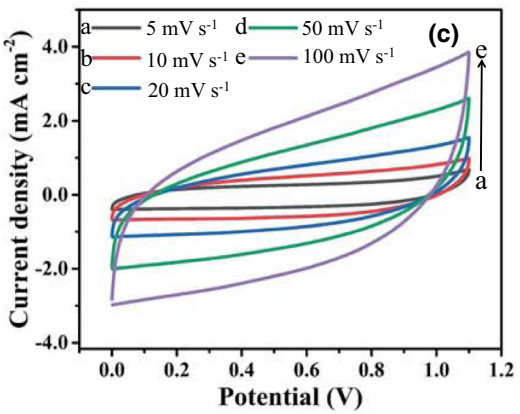
(c)
a 5 mV s-1
b 10 mV s-1
c 20 mV s-1
d 50 mV s-1
e 100 mV s-1
e → a
Current density (mA cm-2)
Potential (V)

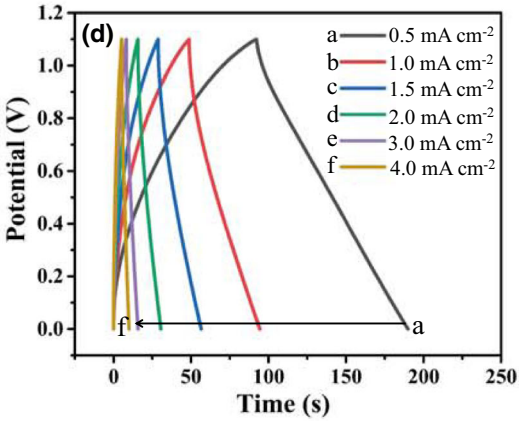
(d)
a 0.5 mA cm-2
b 1.0 mA cm-2
c 1.5 mA cm-2
d 2.0 mA cm-2
e 3.0 mA cm-2
f 4.0 mA cm-2
f → a
Potential (V)
Time (s)

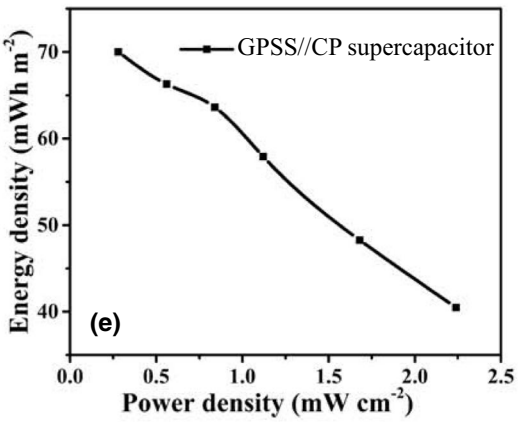
GPSS//CP supercapacitor
(e)
Energy density (mWh m-2)
Power density (mW cm-2)

(f)

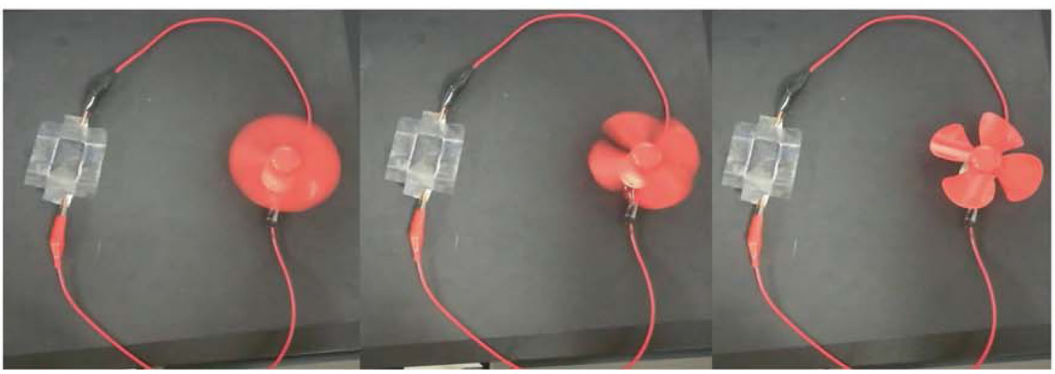

◀**Fig. 8** Electrochemical performance of GPSS//CP supercapacitor: **a** CV curves at the scan rate of 5 mV $s^{-1}$ and **b** GCD curves at 1.0 mA $cm^{-2}$ and an expanded voltage from 0.8 to 1.2 V. **c** CV curves and **d** GCD curves at the voltage of 0–1.1 V. **e** Ragone plot; **f** photographs of its powering electric fan

So, EDX and Raman spectra prove the coating formation of GPSS gel polymer on CP.

## Ionic conductivity of gel polymer

The ionic conductivity of gel polymer electrolyte plays an important role in supercapacitor performance, which is associated with the ion transport. Figure 5a shows the schematic illustrating hydrogen-bonding interaction between GO and PVA. GO involves the hydroxyl groups and epoxy groups on both sides and the carboxyl groups on the edges in the graphite flakes, which can form hydrogen bond with the hydroxyl groups of PVA [38]. Figure 5b shows the schematic illustrating ion transport mechanism in PVA-$Na_2SO_4$ gel polymer electrolyte with different loading mass ratios of GO. The ion transport abides by random walk model characteristic in PVA-$Na_2SO_4$ gel polymer electrolyte, lowing the ion transport efficiency and ionic conductivity as well. GO with two-dimensional layer structure can disperse in PVA matrix to construct the layered channel pathway, shortening the electrolyte ion transport distance. The GO can act as the role of the channeler to facilitate effective ion transport. However, high loading amount of GO may cause the overlapping aggregation of GO nanosheets, leading to the cross-stacking and blocking steric effects [38, 45]. It accordingly causes the decrease of the ionic conductivity of PVA-$Na_2SO_4$ gel polymer electrolyte. So, the loading mass of GO highly affects the electrochemical performance.

The dependence of GO mass concentration on the ionic conductivity of GPSS is fully investigated. Figure 6 shows the ionic conductivity and effective ion transport pathway of GPSS gel polymer electrolyte with different GO mass ratios. Generally, shorter distance of ion transport pathway leads to higher ionic conductivity. The ionic conductivity curve of GPSS exhibits two extremum peaks along with the continuous increase of GO concentration, which is mostly related to the stacking structure of GO sheets. The appropriate incorporation of GO can enhance the ionic conductivity of GPSS gel polymer electrolyte. Its optimal high value of GPSS is 28.86 mS $cm^{-1}$ at GO mass ratio of 0.6% in PVA. The low value of GPSS is 2.99 mS $cm^{-1}$ at GO mass ratio of 1.2%, which is even below 4.33 mS $cm^{-1}$ of PSS. It indicates that the excessive loading mass of GO could cause the cross-stacking effect, which hinders ion transport pathway and lowering the ionic conductivity.

**Table 1** Specific capacitance, power density, and energy density of GPSS//CP supercapacitor at 1.0 mA $cm^{-2}$ and an expanded voltage from 0.8 to 1.2 V

| Voltage (V) | 0.8 | 0.9 | 1.0 | 1.1 | 1.2 |
|---|---|---|---|---|---|
| Specific capacitance (mF $cm^{-2}$) | 27.51 | 31.11 | 35.60 | 39.45 | 50.25 |
| Power density (mW $cm^{-2}$) | 0.40 | 0.45 | 0.50 | 0.55 | 0.60 |
| Energy density (mWh $m^{-2}$) | 24.45 | 34.99 | 49.44 | 66.29 | 100.50 |

## Electrochemical properties

The electrochemical performance of CP supercapacitor with different GO mass ratios in GPSS gel polymer electrolyte is investigated. Figure 7a shows CV curves of CP supercapacitors using GPSS at a scan rate of 10 mV $s^{-1}$. It did not show obvious redox peaks regardless of GO mass ratio in GPSS. Herein, PVA is used as polymer matrix. Layer-structured GO acts as a channeler to direct effective ion transport. $Na_2SO_4$ acts as the supporting electrolyte to improve ionic strength. $Na_2MoO_4$ acts as an electroactive electrolyte to occur the redox reaction of $[Mo(VI)O_4]^{2-}/[Mo(IV)O_3]^{2-}$. Generally, $Na_2MoO_4$ conducts the redox reaction in acidic medium to achieve higher redox activity than that in neutral medium [30, 32]. Herein, the carboxyl group in GO can exist in the form of $COO^-$ and $H^+$ [46]. The $H^+$ can accelerate the redox reaction of $Na_2MoO_4$. The possible reaction mechanism of redox electrolyte of GO/$Na_2MoO_4$ is proposed as follows [47, 48].

$$Mo(VI)O_4^{2-}+2H^+ \leftrightarrows H_2Mo(VI)O_4 \quad (8)$$

$$H_2Mo(VI)O_4+2e^-+2H^+ \leftrightarrows H_2Mo(IV)O_3+H_2O \quad (9)$$

$$H_2Mo(VI)O_4+e^-+H^+ \leftrightarrows HMo(V)O_3+H_2O \quad (10)$$

Figure 7b shows GCD curves of GPSS//CP supercapacitor with different GO mass ratios at 0.5 mA $cm^{-2}$. All GCD curves show symmetric triangular shape, indicating good reversibility. The specific capacitance of CP supercapacitors using GPSS1, GPSS2, GPSS3, GPSS4, GPSS5, and GPSS6 is 31.21, 37.75, 41.67, 31.25, 36.38, and 26.42 mF $cm^{-2}$, respectively. Figure 7c shows the capacitance curve in terms of GO mass ratio in GPSS. The maximum capacitance based on CV and GCD measurement is achieved at the GO mass ratio of 0.65% and 0.59%, respectively. The result is consistent with that of ionic conductivity. Herein, the optimal GO mass ratio is controlled to 0.6% in PVA, which is regarded as the suitable gel polymer electrolyte. It is denoted as GPSS in the following measurement.

Figure 8 a and b show CV curves at 5 mV $s^{-1}$ and GCD curves at 1.0 mA $cm^{-2}$ of GPSS//CP supercapacitor at an expanded voltage from 0.8 to 1.2 V. CV and GCD curves keep identical shape when the output voltage is extended up to 1.1 V. The polarization becomes obvious when the voltage window is above 1.1 V. So the following electrochemical measurement of GPSS//CP supercapacitor is conducted at a voltage window of 1.1 V. Table 1 lists specific capacitance, power density, and energy density of GPSS//CP supercapacitor at 1.0 mA $cm^{-2}$ and an expanded voltage from 0.8 to 1.2 V. The specific capacitance increases from 27.51 to

**Table 2** Specific capacitance, power density, and energy density of GPSS//CP supercapacitor at the voltage of 1.1 V at different current densities

| Current densities (mA $cm^{-2}$) | 0.5 | 1.0 | 1.5 | 2.0 | 3.0 | 4.0 |
|---|---|---|---|---|---|---|
| Specific capacitance (mF $cm^{-2}$) | 41.67 | 39.45 | 37.85 | 34.47 | 28.73 | 24.09 |
| Power density (mW $cm^{-2}$) | 0.28 | 0.55 | 0.83 | 1.10 | 1.65 | 2.20 |
| Energy density (mWh $m^{-2}$) | 70.02 | 66.29 | 63.61 | 57.93 | 48.28 | 40.48 |

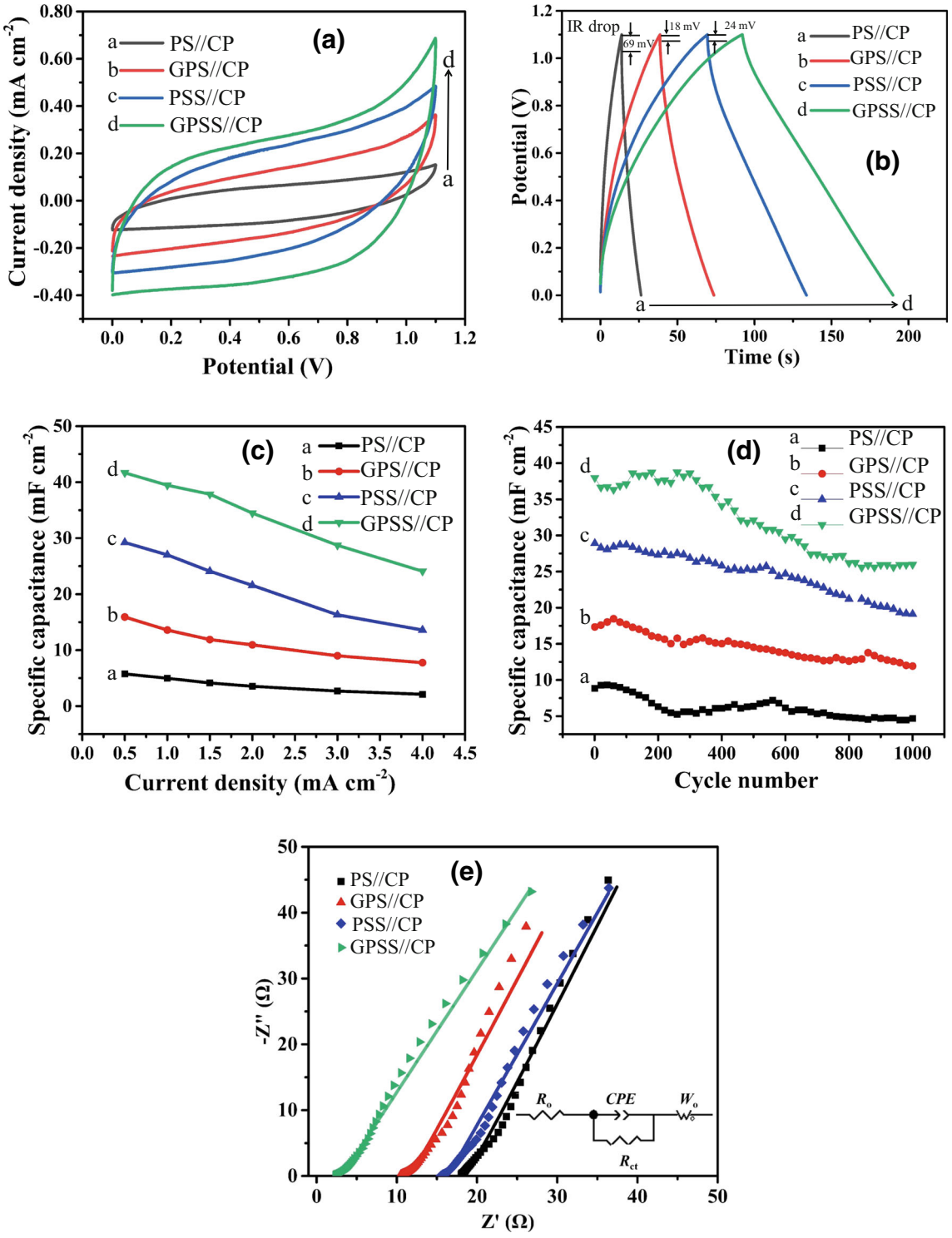

◀ **Fig. 9** Electrochemical performance of PS//CP, GPS//CP, PSS//CP, and GPSS//CP supercapacitors: **a** CV curves at the scan rate of 5 mV $s^{-1}$; **b** GCD curves at 0.5 mA $cm^{-2}$ and the voltage of 1.1 V; **c** rate capacitance retention curves; **d** cycling capacitance retention curves at 0.5 mA $cm^{-2}$; **e** Nyquist plots and fitting curves

50.25 mF $cm^{-2}$ and the energy density increases from 24.45 to 100.50 mWh $m^{-2}$ with the increase of voltage window from 0.8 to 1.2 V. Figure 8 c and d display CV curves and GCD curves of GPSS//CP supercapacitor. CV curves at different scan rates and GCD curves at different densities keep the identical shape, revealing good electrochemical reversibility at a voltage window of 1.1 V. Table 2 lists specific capacitance, power density, and energy density of GPSS//CP supercapacitor at different current densities and the voltage of 1.1 V. When the current density increases from 0.5 to 4 mA $cm^{-2}$, the specific capacitance declines from 41.67 to 24.09 mF $cm^{-2}$, demonstrating the rate capacitance retention of 57.81%. The corresponding energy density declines from 70.02 to 40.48 mWh $m^{-2}$. Figure 8e shows the Ragone plot of specific energy versus specific power for GPSS//CP supercapacitor. The energy density decreases from 70.02 mWh $m^{-2}$ at 0.5 mA $cm^{-2}$ to 40.48 mWh $m^{-2}$ at 4.0 mA $cm^{-2}$. Figure 8f shows photographs of GPSS//CP supercapacitor powering electric device. This supercapacitor with effective working dimension of 3 × 2 × 0.3 cm can continuously power electric fan for 35 s when it is charged.

Electrochemical performance is investigated for PS//CP, GPS//CP, PSS//CP, and GPSS//CP supercapacitor. Figure 9 a and b show CV curves at the same scan rate of 5 mV $s^{-1}$ and GCD curves at 0.5 mA $cm^{-2}$ and the voltage of 1.1 V. The integral CV area follows the order of PS < GPS < PSS < GPSS. The GCD curves show a good reversibility at the voltage of 1.1 V. The specific capacitance of PS//CP, GPS//CP, PSS//CP, and GPSS//CP supercapacitor is 5.53, 15.91, 29.23, and 41.67 mF $cm^{-2}$ at 0.5 mA $cm^{-2}$. The GO in GPS and GPSS could act as ion transport channeler to improve ionic conductivity and capacitance performance of CP supercapacitor. The reactive $Na_2MoO_4$ in PSS and GPSS could act as the redox electrolyte to introduce additional Faradic capacitance. The $Na_2MoO_4$ takes more effective role than GO. Figure 9c shows the rate capacitance retention curves. The PSS//CP supercapacitor keeps the areal specific capacitance of 29.23 mF $cm^{-2}$. This result is much higher than 5.53 mF $cm^{-2}$ of PS//CP supercapacitor at 0.5 mA $cm^{-2}$, but a little lower than 38.2 mF $cm^{-2}$ for PVA-$H_3PO_4$-$Na_2MoO_4$// graphene supercapacitor [30]. Electroactive $Na_2MoO_4$ electrolyte conducts redox reaction to provide pseudocapacitanc in $Na_2SO_4$ medium, causing the improved capacitance than that in the absence of $Na_2MoO_4$. Noticeably, the redox activity of $Na_2MoO_4$ electrolyte is lower in neural $Na_2SO_4$ medium than that in acidic medium, causing the declined pseudocapacitance. The $IR_{drop}$ decreases obviously from 69 mV of PS//CP, 18 mV of GPS//CP, and 24 mV of PSS// CP to a negligible level of GPSS//CP. The ESR is also decreases from 69 Ω $cm^{-2}$ of PS//CP, 18 Ω $cm^{-2}$ of GPS//CP, and 24 Ω $cm^{-2}$ of PSS//CP to the negligible level of GPSS//CP. It indicates that GPSS//CP supercapacitor has high charge transfer capability. Figure 9d shows the cycling performance of PS//CP, GPS//CP, PSS//CP, and GPSS//CP supercapacitors at 0.5 mA $cm^{-2}$ for 1000 cycles. The cycling capacitance retention of GPSS//CP supercapacitor is 71%, which is higher than 69% for PSS//CP, 68% for GPS//CP, and 56% for PS//CP supercapacitors. It indicates the superior cycling stability of GPSS//CP supercapacitor.

The EIS measurements are conducted for PS//CP, GPS//CP, PSS//CP, and GPSS//CP supercapacitors. The corresponding Nyquist plots and fitting curves are displayed in Fig. 9e. The equivalent circuit model includes Ohm resistance ($R_o$), charge transfer resistance ($R_{ct}$), constant phase element ($CPE$), and Warburg resistance ($W_o$). Table 3 lists the fitting values of equivalent circuit elements. According to Eq. (5), the effective diffusion coefficient ($D$) is 0.04, 0.09, 0.03, and 0.08, respectively. Obviously, the GO could promote the ion diffusion in both PS and PSS gel polymer electrolyte. All the plots include a not obvious semicircle at high frequencies and a straight line at the low frequencies. The $R_o$ is the internal resistance, which is calculated from the intersection of the plot on the $x$-axis in the high frequency region and related to the electrolyte ion resistance and intrinsic resistance of the carbon paper electrode. The $R_o$ is 10.32 Ω for GPS///CP and 2.31 Ω for GPSS//CP, which is lower than 17.89 Ω for PS//CP and 15.38 Ω for PSS//CP. The $R_{ct}$ is the charge transfer resistance, which is associated with the charge transfer process at the electrolyte and electrode interface. The $R_{ct}$ is 0.84 Ω for

**Table 3** Fitting values of equivalent circuit elements of PS//CP, GPS//CP, PSS//CP, and GPSS//CP supercapacitors

| Gel polymer electrolyte | $R_o$ (Ω) | $R_{ct}$ (Ω) | $CPE$ | | $W_o$ | | |
|---|---|---|---|---|---|---|---|
| | | | $CPE_T$ | $CPE_P$ | $W_R$ (Ω) | $W_T$ | $W_P$ |
| PS | 17.89 | 1.38 | 0.01 | 0.56 | 2.85 | 25.71 | 0.74 |
| GPS | 10.32 | 0.73 | 0.02 | 0.66 | 1.95 | 11.01 | 0.74 |
| PSS | 15.38 | 1.62 | 0.02 | 0.60 | 3.02 | 30.09 | 0.68 |
| GPSS | 2.31 | 0.84 | 0.04 | 0.63 | 2.48 | 13.39 | 0.69 |

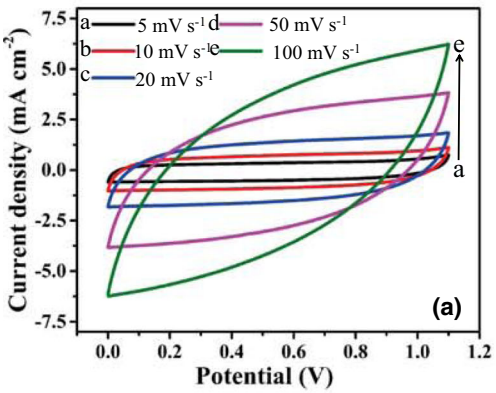
a 5 mV s-1
b 10 mV s-1
c 20 mV s-1
d 50 mV s-1
e 100 mV s-1
Current density (mA cm-2)
Potential (V)
(a)

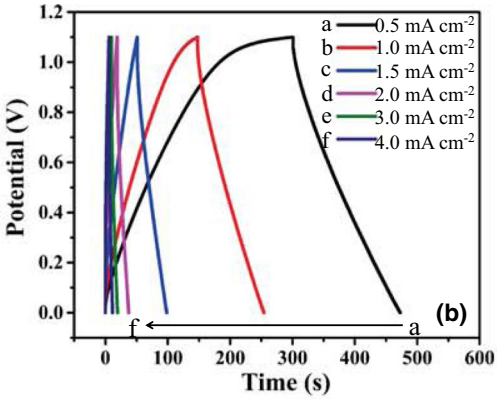
a 0.5 mA cm-2
b 1.0 mA cm-2
c 1.5 mA cm-2
d 2.0 mA cm-2
e 3.0 mA cm-2
f 4.0 mA cm-2
Potential (V)
Time (s)
(b)

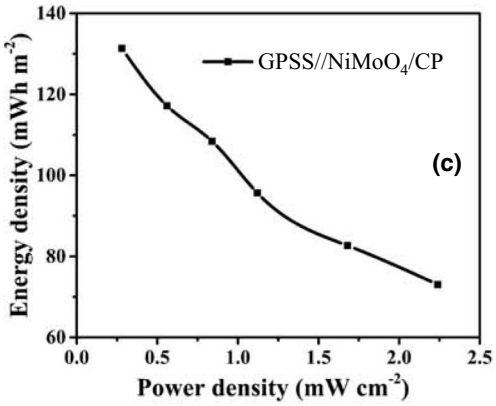
GPSS//NiMoO4/CP
Energy density (mWh m-2)
Power density (mW cm-2)
(c)

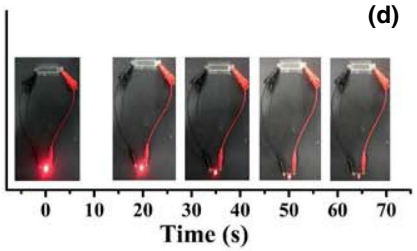
(d)
Time (s)

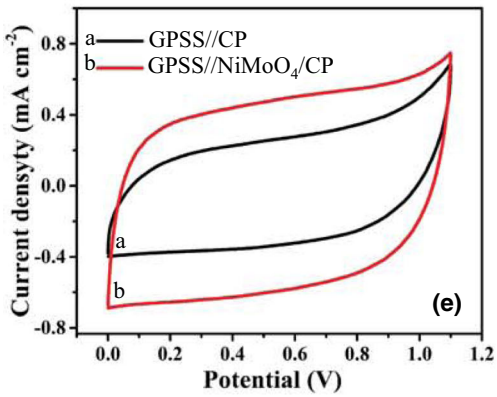
a GPSS//CP
b GPSS//NiMoO4/CP
Current densyty (mA cm-2)
Potential (V)
(e)

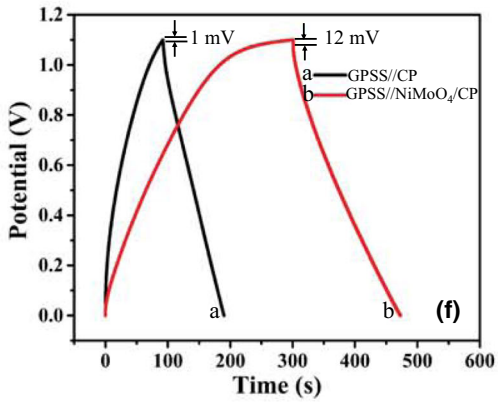
1 mV
12 mV
a GPSS//CP
b GPSS//NiMoO4/CP
Potential (V)
Time (s)
(f)

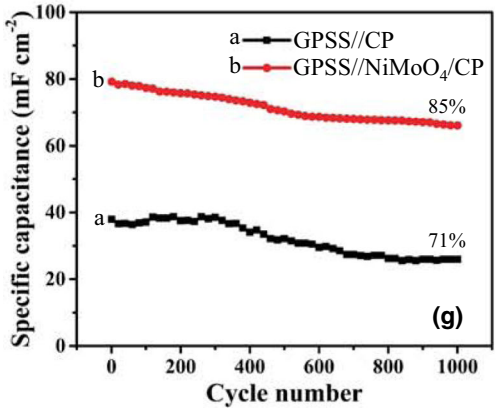
a GPSS//CP
b GPSS//NiMoO4/CP
85%
71%
Specific capacitance (mF cm-2)
Cycle number
(g)

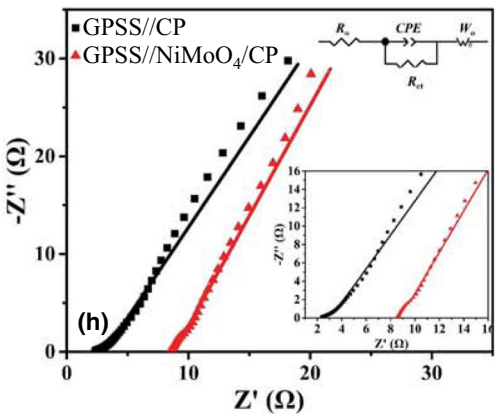
GPSS//CP
GPSS//NiMoO4/CP
-Z'' (Ω)
Z' (Ω)
(h)

◀**Fig. 10** Electrochemical performance of GPSS//$NiMoO_4$/CP supercapacitor: **a** CV curves and **b** GCD curves at the voltage of 1.1 V, **c** Ragone plot; **d** photographs of the discharge time duration of powering LED luminance; electrochemical performance of GPSS//CP and GPSS//$NiMoO_4$/CP supercapacitors: **e** CV curves at a scan rate of 5 mV $s^{-1}$, **f** GCD curves at 0.5 mA $cm^{-2}$ and the voltage window of 1.1 V, **g** cycling capacitance retention curves at 0.5 mA $cm^{-2}$ for 1000 cycles, **h** Nyquist plots and fitting curves (the inset shows the equivalent circuit and the enlarged Nyquist plots at the high frequency region)

GPSS//CP, which is lower than 1.38 Ω for PS//CP and 1.62 Ω for PSS//CP, but slightly higher than 0.73 Ω for GPS//CP. The GO can effectively shorten the electrolyte ion transport pathway. CPE consists of two parameters of $CPE_T$ and $CPE_p$. $CPE_T$ is the double layer constant phase element, which is an indicator of the double layer capacitance between the electrode and the electrolyte. The $CPE_T$ for GPSS//CP is higher than others, presenting higher double layer capacitance. $CPE_P$ is the constant phase element exponent between 0 and 1. The higher $CPE_p$ value presents that the supercapacitor is closer to ideal capacitor. The $CPE_p$ is 0.63 for GPSS//CP, which is higher than 0.56 for PS//CP and 0.60 for PSS//CP, but slightly lower than 0.66 for GPS//CP. Furthermore, $W_R$ is the Warburg diffusion resistance, which is related to the diffusion of electrolyte ions in the gel polymer electrolyte and electrode. It can be observed from the slope of the lines in the low frequency range. The $W_R$ is lowered from 2.85 Ω for PS//CP to 1.95 Ω for GPS//CP and from 3.02 Ω for PSS//CP to 2.48 Ω for GPSS//CP. It indicates that GO contributes to improving ion diffusion behavior. The straight lines for PSS//CP and GPSS//CP are deviated when compared with that for PS//CP and GPS//CP, which confirms the presence of pseudocapacitive nature [30]. The tendency of $W_R$ value is consistent with that of $D$ value. So, the GPSS//CP supercapacitor exhibits the superior electrochemical capacitor behavior.

The redox active electrolyte contributes to the limited enhancement of pseudocapacitance for CP supercapacitor. Comparatively, the redox active electrode could more obviously enhance pseudocapacitance. In order to improve the electrochemical performance, the GPSS//$NiMoO_4$/CP supercapacitor is constructed and its electrochemical performance is investigated for the comparison with GPSS//CP supercapacitor. Figure 10 a and b show CV curves at different scan rates and GCD curves at different current densities of GPSS//$NiMoO_4$/CP supercapacitor at the voltage window of 1.1 V. Table 4 lists the corresponding specific capacitance, power density, and energy density of GPSS//$NiMoO_4$/CP supercapacitor. The GPSS//$NiMoO_4$/CP supercapacitor shows higher capacitance than that of GPSS//CP supercapacitor at the same current density. This is ascribed to the pseudocapacitance originated from $NiMoO_4$. Fig. 10c shows the Ragone plot of GPSS//$NiMoO_4$/CP supercapacitor. The energy density decreases from 131.39 mWh $m^{-2}$ at 0.5 mA $cm^{-2}$ to 73.05 mWh $m^{-2}$ at 4.0 mA $cm^{-2}$. Figure 11d shows the photographs of the discharge time duration of LED luminance powered by GPSS//$NiMoO_4$/CP supercapacitor. This supercapacitor can continuously power LED for 60 s. Figure 10 e and f show CV curves at a scan rate of 5 mV $s^{-1}$ and GCD curves at 0.5 mA $cm^{-2}$ and the voltage window of 1.1 V for the GPSS//CP and GPSS//$NiMoO_4$/CP supercapacitors. The current response and integral area of CV curves for GPSS//$NiMoO_4$/CP supercapacitor are larger than that for GPSS//CP supercapacitor at the same scan rate. The discharge time of GPSS//$NiMoO_4$/CP supercapacitor is much larger than that of GPSS//CP supercapacitor at the same current density. It indicates higher electrochemical performance of GPSS//$NiMoO_4$/CP. Normally, $NiMoO_4$ can conduct Faradic redox reaction based on nickel and molybdenum elements in different electrolytes. Herein, the reversible redox reaction [$Ni(II) \rightleftharpoons Ni(III) + e^-$] in neural $Na_2SO_4$ medium is mainly occurred to introduce extra pseudocapacitance for GPSS//$NiMoO_4$/CP supercapacitor [49, 50]. The $IR_{drop}$ of GPSS//$NiMoO_4$/CP supercapacitor is a little bigger than that of GPSS//CP supercapacitor. The intrinsic resistance of $NiMoO_4$ lowers electrical conductivity of GPSS//$NiMoO_4$/CP supercapacitor. Figure 10g shows the cycling performance of GPSS//$NiMoO_4$/CP supercapacitor at 0.5 mA $cm^{-2}$ for 1000 cycles. The cycling capacitance retention of GPSS//$NiMoO_4$/CP supercapacitor retains 85%, which is higher than 71% for GPSS//CP supercapacitor. Figure 10h shows Nyquist plots and fitting curves for GPSS//CP and GPSS//$NiMoO_4$/CP supercapacitors. The inset shows the equivalent circuit and the enlarged Nyquist plots at the high frequency region. Table 5 lists the fitting values of the equivalent circuit elements of GPSS//CP and GPSS//$NiMoO_4$/CP supercapacitors. The $R_o$ increases from 2.31 Ω for GPSS///CP to 8.44 Ω for GPSS//$NiMoO_4$ CP, presenting the higher intrinsic Ohmic resistance of GPSS//$NiMoO_4$/CP supercapacitor. The $R_{ct}$ also increases from 0.84 Ω for GPSS//CP to 3.21 Ω

**Table 4** Specific capacitance, power density, and energy density of GPSS//$NiMoO_4$/CP supercapacitor at the voltage of 1.1 V at different current densities

| Current densities (mA $cm^{-2}$) | 0.5 | 1.0 | 1.5 | 2.0 | 3.0 | 4.0 |
|---|---|---|---|---|---|---|
| Specific capacitance (mF $cm^{-2}$) | 78.18 | 69.73 | 64.50 | 56.93 | 49.18 | 43.47 |
| Power density (mW $cm^{-2}$) | 0.28 | 0.55 | 0.83 | 1.10 | 1.65 | 2.20 |
| Energy density (mWh $m^{-2}$) | 131.39 | 117.19 | 108.40 | 95.67 | 82.65 | 73.05 |

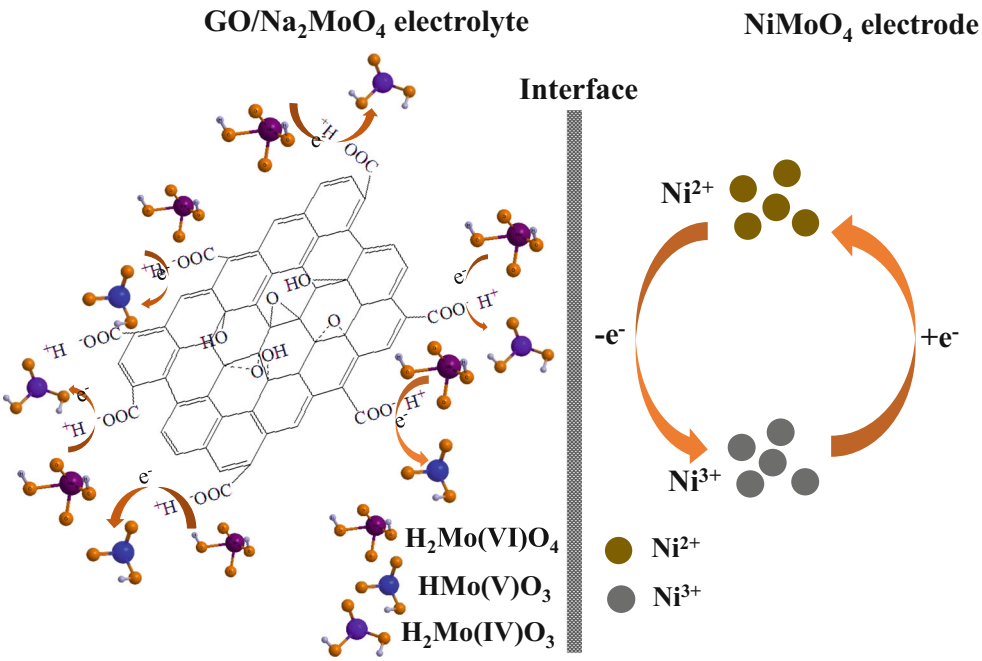


**Fig. 11** Schematic showing reversible Faradaic reaction in $GO/Na_2MoO_4$ electrolyte and at $NiMoO_4$ electrode

for GPSS//$NiMoO_4$/CP, presenting higher charge transfer resistance of GPSS//$NiMoO_4$/CP supercapacitor. The higher $R_o$ and $R_{ct}$ values are related to the low electrical conductivity of $NiMoO_4$ [51, 52]. This result is consistent with the $IR_{drop}$ shown in Fig. 9b. The $CPE_T$ increases from 0.04 for GPSS//CP to 0.05 for GPSS//$NiMoO_4$/CP, presenting its higher double layer capacitance. The $CPE_p$ increases from 0.63 for GPSS//$NiMoO_4$/CP to 0.75 for GPSS//CP, presenting its more approaching to capacitor behavior. The $W_R$ decreases from 2.48 Ω for GPSS//CP to 1.67 Ω for GPSS//$NiMoO_4$/CP, presenting its more feasible electrolyte ion diffusion.

Figure 11 shows the schematic of Faradaic reaction for $Na_2MoO_4$ electrolyte and $NiMoO_4$ electrode. The enhanced capacitance originates from the redox reaction of both redox $NiMoO_4$ electrode and redox $Na_2MoO_4$ electrolyte. High performance of GPSS//$NiMoO_4$/CP supercapacitor is ascribed to the following reasons. Firstly, GO in GPSS gel polymer electrolyte can introduce free channel in gel polymer to promote ion transport. It shortens ion transfer pathway and then improves the ionic conductivity of gel polymer electrolyte. Secondly, the redox reaction of Mo(VI)/Mo(V) and Mo(VI)/Mo(IV) is occurred on GO in GPSS electrolyte, which is shown as $H_2Mo(VI)O_4 + 2e^- + 2H^+ \leftrightarrows H_2Mo(IV)O_3 + H_2O$ with a redox potential of 0.24/0.55 V vs SHE and $H_2Mo(VI)O_4 + e^- + H^+ \leftrightarrows HMo(V)O_3 + H_2O$ with a redox potential of 0.69/0.29 V vs SHE [31, 53]. The redox reaction of Ni(II)/Ni(III) is occurred on $NiMoO_4$/CP electrode, which is shown as $Ni^{2+} \leftrightarrows Ni^{3+} + e^-$ with a redox potential of 0.70/0.45 V vs SHE [50]. In the charge–discharge process of GPSS//$NiMoO_4$/CP supercapacitor, the redox reaction of Mo(VI)/Mo(IV) is occurred preferentially on the edge of GO with the carboxyl-ionized proton in the $GO/Na_2MoO_4$ electrolyte. The redox reaction of $Ni^{2+}$ is occurred at the $NiMoO_4$ electrode. Redox electroactive $GO/Na_2MoO_4$ gel electrolyte and $NiMoO_4$ electrode are integrated to fabricate CP supercapacitor to improve capacitance performance.

Table 6 shows the comparison of electrochemical performance for supercapacitors using the gel polymer electrolytes. In comparison with the supercapacitors using various carbon or graphene electrode and GO or $Na_2MoO_4$ gel electrolyte, the GPSS//CP supercapacitor shows the similar or even better electrochemical performance in $Na_2SO_4$ medium when GO and $Na_2MoO_4$ are used in gel polymer electrolyte. In addition, the as-reported $Na_2MoO_4$ gel polymer electrolyte is usually applied to coat carbon electrode to construct supercapacitors. Redox $Na_2MoO_4$ gel polymer electrolyte and redox $NiMoO_4$

**Table 5** Fitting values of the equivalent circuit elements of GPSS//CP and GPSS//$NiMoO_4$/CP supercapacitors

| Supercapacitor | $R_o$ (Ω) | $R_{ct}$ (Ω) | *CPE* | | $W_o$ | | |
|---|---|---|---|---|---|---|---|
| | | | $CPE_T$ | $CPE_P$ | $W_R$ (Ω) | $W_T$ | $W_P$ |
| GPSS//CP | 2.31 | 0.84 | 0.04 | 0.63 | 2.48 | 13.39 | 0.69 |
| GPSS//$NiMoO_4$/CP | 8.44 | 3.21 | 0.05 | 0.75 | 1.67 | 18.87 | 0.67 |

**Table 6** Comparison of electrochemical performance of supercapacitors using gel polymer electrolytes

| Electrode material | Electrolyte | Specific capacitance | Energy density | Reference |
|---|---|---|---|---|
| rGO nanosheets | PVA-$H_3PO_4$-$Na_2MoO_4$ | 38.2 mF $cm^{-2}$ at 0.5 mA $cm^{-2}$ | 53 mWh $m^{-2}$ at 0.5 mA $cm^{-2}$ | [30] |
| Activated carbon | PVA-$H_2SO_4$-$Na_2MoO_4$ | 648 F $g^{-1}$ at 1.56 A $g^{-1}$ | 14.4 Wh $kg^{-1}$ at 1.56 A $g^{-1}$ | [32] |
| Graphene-doped carbon | P(VDF-HFP)-EMIMB$F_4$-GO | 190 F $g^{-1}$ at 1 A $g^{-1}$ | 76 Wh $kg^{-1}$ at 1 A $g^{-1}$ | [54] |
| Activated carbon RP20 | P(VDF-HFP)-EMIMB$F_4$-GO | – | 32.4 Wh $kg^{-1}$ at 10 A $g^{-1}$ | [39] |
| Activated carbon | GO-B-PVA/KOH | 141.8 F $g^{-1}$ at 0.1 A $g^{-1}$ | – | [38] |
| 70(70PEO:30AgI):30 AC | 93(70PEO:30AgI):7$Al_2O_3$ | 2.5 F $g^{-1}$ at 0.05 A $g^{-1}$ | – | [55] |
| Sn-$LiCoPO_4$ | LiOH aqueous solution | 80 mAh $g^{-1}$ | – | [56] |
| 70(70PEO:30AgI): 30 AC | 95(70PEO:30AgI):5$SiO_2$ | 20 F $g^{-1}$ at 0.4 A $g^{-1}$ | – | [57] |
| Carbon paper | GO/PVA-$Na_2SO_4$-$Na_2MoO_4$ | 41.67 mF $cm^{-2}$ at 0.5 mA $cm^{-2}$ | 73.34 mWh $m^{-2}$ at 0.5 mA $cm^{-2}$ | This work |
| $NiMoO_4$/carbon paper | GO/PVA-$Na_2SO_4$-$Na_2MoO_4$ | 78.18 mF $cm^{-2}$ at 0.5 mA $cm^{-2}$ | 9 mWh $m^{-2}$ at 0.5 mA $cm^{-2}$ | This work |

electrode are seldom integrated in the same supercapacitor system. Significantly, the redox reaction of both electrolyte and electrode is simultaneously introduced in GPSS//$NiMoO_4$/CP supercapacitor. It shows the specific capacitance of 78.18 mF $cm^{-2}$ and energy density of 131.39 mWh $m^{-2}$ at 0.5 mA $cm^{-2}$. So, the GPSS gel polymer electrolyte and $NiMoO_4$/CP electrode are promising candidates for supercapacitors application.

## Conclusions

The GO/PVA-$Na_2SO_4$-$Na_2MoO_4$ (GPSS) gel polymer electrolyte and $NiMoO_4$/CP electrode are used to prepare high-performance supercapacitor. Owing to the effective ion transport pathway provided by GO in polymer gel electrolyte, the ionic conductivity increases from 3.73 mS $cm^{-1}$ for PVA-$Na_2SO_4$ (PS) to 6.46 mS $cm^{-1}$ for GO/PVA-$Na_2SO_4$ (GPS) at optimal GO mass ratio of 0.6% in PVA gel. The ionic conductivity even highly increases from 4.33 mS $cm^{-1}$ for PVA-$Na_2SO_4$-$Na_2MoO_4$ (PSS) gel to 28.86 mS $cm^{-1}$ for GO/PVA-$Na_2SO_4$-$Na_2MoO_4$ (GPSS) gel. The GPSS//CP supercapacitor shows specific capacitance of 41.67 mF $cm^{-2}$ and energy density of 70.02 mWh $m^{-2}$ at 0.5 mA $cm^{-2}$, which is higher than 15.91 mF $cm^{-2}$ and 26.74 mWh $m^{-2}$ for the GPS//CP supercapacitor. The GPSS//$NiMoO_4$/CP supercapacitor shows even higher specific capacitance of 78.18 mF $cm^{-2}$ and energy density of 131.39 mWh $m^{-2}$ at 0.5 mA $cm^{-2}$, which is ascribed to the pseudocapacitance provided the reversible redox reaction of Mo(VI)/Mo(V), Mo(VI)/Mo(IV), and Ni(II)/Ni(III). It also shows high cycling capacitance retention of 85% at 0.5 mA $cm^{-2}$ for 1000 cycles. The GPSS//$NiMoO_4$/CP supercapacitor is desirable for the promising application in energy storage devices.

**Funding information** The work was financially supported by the National Natural Science Foundation of China (no. 21373047), Graduate Innovation Program of Jiangsu Province (KYCX18_0080), the Fundamental Research Funds for the Central Universities (2242018K41024), and the Priority Academic Program Development of Jiangsu Higher Education Institutions.

## References

1. Lu X, Yu M, Wang G, Tong Y, Li Y (2014) Flexible solid-state supercapacitors: design, fabrication and applications. Energy Environ Sci 7:2160–2181
2. Xie Y (2019) Electrochemical performance of transition metal-coordinated polypyrrole: A Mini Review. Chem Rec 19:1–16
3. Zhao Z, Xie Y, Lu L (2018) Electrochemical performance of polyaniline-derivated nitrogen-doped carbon nanowires. Electrochim Acta 283:1618–1631
4. Zhao Z, Xie Y (2018) Electrochemical supercapacitor performance of boron and nitrogen co-doped porous carbon nanowires. J Power Sources 400:264–276
5. Zhou Y, Xie Y (2018) Enhanced electrochemical stability of carbon quantum dots-incorporated and ferrous-coordinated polypyrrole for supercapacitor. J Solid State Electrochem 22:2515–2529
6. Xie Y, Zhou Y (2018) Enhanced electrochemical stability of CuCo bimetallic-coordinated polypyrrole. Electrochim Acta 290:419–428
7. Xie Y, Sha X (2018) Electrochemical cycling stability of nickel (II) coordinated polyaniline. Synth Met 237:29–39
8. Lu L, Xie Y (2019) Phosphomolybdic acid cluster bridging carbon dots and polyaniline nanofibers for effective electrochemical energy storage. J Mater Sci 54:4842–4858
9. Xie Y, Sun P (2018) Electrochemical performance of interspace-expanded molybdenum disulfide few-layer. J Nanopart Res 20:183
10. Eskusson J, Rauwel P, Nerut J, Janes A (2016) A Hybrid Capacitor Based on Fe3O4-Graphene Nanocomposite/Few-Layer Graphene in Different Aqueous Electrolytes. J Electrochem Soc 163:A2768–A2775
11. Hu S, Ribeiro EL, Davari SA, Tian M, Mukherjee D, Khomami B (2017) Hybrid nanocomposites of nanostructured Co3O4 interfaced with reduced/nitrogen-doped graphene oxides for selective improvements in electrocatalytic and/or supercapacitive properties. RSC Adv 7:33166–33176
12. Li Z, Zhang W, Liu Y, Guo J, Yang B (2018) 2D nickel oxide nanosheets with highly porous structure for high performance capacitive energy storage. J Phys D: Appl Phys 51:045302
13. Gao Z, Yang WL, Wang J, Song NN, Li XD (2015) Flexible all-solid-state hierarchical NiCo2O4/porous graphene paper asymmetric supercapacitors with an exceptional combination of electrochemical properties. Nano Energy 13:306–317

14. Chen YP, Liu BR, Liu Q, Wang J, Li ZS, Jing XY, Liu LH (2015) Coaxial CoMoO4 nanowire arrays with chemically integrated conductive coating for high-performance flexible all-solid-state asymmetric supercapacitors. Nanoscale 7:15159–15167
15. Watcharatharapong T, Sundaram MM, Chakraborty S, Li D, Shafiullah G, Aughterson RD, Ahuja R (2017) Effect of Transition Metal Cations on Stability Enhancement for Molybdate-Based Hybrid Supercapacitor. Acs Appl Mater Interface 9:17977–17991
16. Lu L, Xie Y, Zhao Z (2018) Improved electrochemical stability of NixCo2x(OH)(6x)/NiCo2O4 electrode material. J Alloys Compd 731:903–913
17. Kumar Y, Pandey GP, Hashmi SA (2012) Gel Polymer Electrolyte Based Electrical Double Layer Capacitors: Comparative Study with Multiwalled Carbon Nanotubes and Activated Carbon Electrodes. J Phys Chem C 116:26118–26127
18. Fernicola A, Weise FC, Greenbaum SG, Kagimoto J, Scrosati B, Soleto A (2009) Lithium-Ion-Conducting Electrolytes: From an Ionic Liquid to the Polymer Membrane. J Electrochem Soc 156: A514–A520
19. Wang P, Zakeeruddin SM, Moser JE, Nazeeruddin MK, Sekiguchi T, Gratzel M (2003) A stable quasi-solid-state dye-sensitized solar cell with an amphiphilic ruthenium sensitizer and polymer gel electrolyte. Nat Mater 2:402–407
20. Verma P, Maire P, Novak P (2010) A review of the features and analyses of the solid electrolyte interphase in Li-ion batteries. Electrochim Acta 55:6332–6341
21. Hashmi SA, Latham RJ, Linford RG, Schlindwein WS (1998) Conducting polymer-based electrochemical redox supercapacitors using proton and lithium ion conducting polymer electrolytes. Polym Int 47:28–33
22. Meng C, Liu C, Chen L, Hu C, Fan S (2010) Highly flexible and all-solid-state paperlike polymer supercapacitors. Nano Lett 10: 4025–4031
23. Yang CC, Hsu ST, Chien WC (2005) All solid-state electric double-layer capacitors based on alkaline polyvinyl alcohol polymer electrolytes. J Power Sources 152:303–310
24. Yang C-C, Wu GM (2009) Study of microporous PVA/PVC composite polymer membrane and it application to MnO2 capacitors. Mater Chem Phys 114:948–955
25. Lewandowski A, Zajder M, Frackowiak E, Beguin F (2001) Supercapacitor based on activated carbon and polyethylene oxide-KOH-H2O polymer electrolyte. Electrochim Acta 46:2777–2780
26. Lee KT, Wu NL (2008) Manganese oxide electrochemical capacitor with potassium poly(acrylate) hydrogel electrolyte. J Power Sources 179:430–434
27. Xie Y, Wang J (2018) Capacitance performance of carbon paper supercapacitor using redox-mediated gel polymer electrolyte. J Sol-Gel Sci Technol 86:760–772
28. Yu H, Wu J, Fan L, Xu K, Zhong X, Lin Y, Lin J (2011) Improvement of the performance for quasi-solid-state supercapacitor by using PVA–KOH–KI polymer gel electrolyte. Electrochim Acta 56:6881–6886
29. Ma G, Li J, Sun K, Peng H, Mu J, Lei Z (2014) High performance solid-state supercapacitor with PVA–KOH–K3[Fe(CN)6] gel polymer as electrolyte and separator. J Power Sources 256:281–287
30. Veerasubramani GK, Krishnamoorthy K, Pazhamalai P, Kim SJ (2016) Enhanced electrochemical performances of graphene based solid-state flexible cable type supercapacitor using redox mediated polymer gel electrolyte. Carbon 105:638–648
31. Xu D, Hu W, Sun XN, Cui P, Chen XY (2017) Redox additives of Na 2 MoO 4 and KI: Synergistic effect and the improved capacitive performances for carbon-based supercapacitors. J Power Sources 341:448–456
32. Senthilkumar ST, Selvan RK, Melo JS, Sanjeeviraja C (2013) High Performance Solid-State Electric Double Layer Capacitor from Redox Mediated Gel Polymer Electrolyte and Renewable Tamarind Fruit Shell Derived Porous Carbon. Acs Appl Mater Interface 5:10541–10550
33. Senthilkumar ST, Selvan ARK, Ponpandian AN, Meloc BJS, Leed YS (2013) Improved performance of electric double layer capacitor using redox additive (VO2+/VO2+) aqueous electrolyte. J Mater Chem A 1:7913–7919
34. Yu H, Wu J, Fan L, Lin Y, Xu K, Tang Z, Cheng C, Tang S, Lin J, Huang M, Lan Z (2012) A novel redox-mediated gel polymer electrolyte for high-performance supercapacitor. J Power Sources 198: 402–407
35. Ma G, Dong M, Sun K, Feng E, Peng H, Lei Z (2015) A redox mediator doped gel polymer as an electrolyte and separator for a high performance solid state supercapacitor. J Mater Chem A 3: 4035–4041
36. Pan S, Deng J, Guan G, Zhang Y, Chen P, Ren J, Peng H (2015) A redox-active gel electrolyte for fiber-shaped supercapacitor with high area specific capacitance. J Mater Chem A 3:6286–6290
37. Sun K, Ran F, Zhao G, Zhu Y, Zheng Y, Ma M, Zheng X, Ma G, Lei Z (2016) High energy density of quasi-solid-state supercapacitor based on redox-mediated gel polymer electrolyte. RSC Adv 6: 55225–55232
38. Huang Y-F, Wu P-F, Zhang M-Q, Ruan W-H, Giannelis EP (2014) Boron cross-linked graphene oxide/polyvinyl alcohol nanocomposite gel electrolyte for flexible solid-state electric double layer capacitor with high performance. Electrochim Acta 132:103–111
39. Yang X, Zhang F, Zhang L, Zhang T, Huang Y, Chen Y (2013) A High-Performance Graphene Oxide-Doped Ion Gel as Gel Polymer Electrolyte for All-Solid-State Supercapacitor Applications. Adv Funct Mater 23:3353–3360
40. Ni Z, Wang Y, Yu T, Shen Z (2008) Raman spectroscopy and imaging of graphene. Nano Res 1:273–291
41. Jothi PR, Kannan S, Velayutham G (2015) Enhanced methanol electro-oxidation over in-situ carbon and graphene supported one dimensional NiMoO4 nanorods. J Power Sources 277:350–359
42. Niyogi S, Bekyarova E, Itkis ME, Zhang H, Shepperd K, Hicks J, Sprinkle M, Berger C, Lau CN, deHeer WA, Conrad EH, Haddon RC (2010) Spectroscopy of Covalently Functionalized Graphene. Nano Lett 10:4061–4066
43. Su CY, Xu YP, Zhang WJ, Zhao JW, Tang XH, Tsai CH, Li LJ (2009) Electrical and Spectroscopic Characterizations of Ultra-Large Reduced Graphene Oxide Monolayers. Chem Mater 21: 5674–5680
44. Reddy BJ, Vickraman P, Justin AS (2019) Synthesis and Characterization of Graphene/Binary Metal Molybdate (Graphene/Zn1-xNixMoO4) Nanocomposite for Supercapacitors. Phys Status Solidi A 216:1800595
45. Ye Y-S, Cheng M-Y, Xie X-L, Rick J, Huang Y-J, Chang F-C, Hwang B-J (2013) Alkali doped polyvinyl alcohol/graphene electrolyte for direct methanol alkaline fuel cells. J Power Sources 239: 424–432
46. Cao Y-C, Xu C, Wu X, Wang X, Xing L, Scott K (2011) A poly (ethylene oxide)/graphene oxide electrolyte membrane for low temperature polymer fuel cells. J Power Sources 196:8377–8382
47. Li WS, Tian LP, Huang QM, Li H, Chen HY, Lian XP (2002) Catalytic oxidation of methanol on molybdate-modified platinum electrode in sulfuric acid solution. J Power Sources 104:281–288
48. Moutarlier V, Gigandet MP, Pagetti J, Ricq L (2003) Molybdate/sulfuric acid anodising of 2024-aluminium alloy: influence of inhibitor concentration on film growth and on corrosion resistance. Surface and Coatings Technology 173:87–95
49. Jothi PR, Shanthi K, Salunkhe RR, Pramanik M, Malgras V, Alshehri SM, Yamauchi Y (2015) Synthesis and Characterization of α-NiMoO4 Nanorods for Supercapacitor Application. Eur J Inorg Chem (22):3694–3699

50. Ramkumar R, Sundaram MM (2016) Electrochemical synthesis of polyaniline crosslinked NiMoO4 nanofibre dendrites for energy storage devices. New J Chem 40:7456–7464
51. Moreno B, Chinarro E, Colomer MT, Jurado JR (2010) Combustion Synthesis and Electrical Behavior of Nanometric β-NiMoO4. J Phys Chem C 114:4251–4257
52. Li P, Ruan C, Xu J, Xie Y (2019) Enhanced capacitive performance of CoO-modified NiMoO4 nanohybrid as advanced electrodes for asymmetric supercapacitor. J Alloys Compd 791:152–165
53. Sun K, Feng E, Peng H, Ma G, Wu Y, Wang H, Lei Z (2015) A simple and high-performance supercapacitor based on nitrogen-doped porous carbon in redox-mediated sodium molybdate electrolyte. Electrochim Acta 158:361–367
54. Yang X, Zhang L, Zhang F, Zhang T, Huang Y, Chen Y (2014) A high-performance all-solid-state supercapacitor with graphene-doped carbon material electrodes and a graphene oxide-doped ion gel electrolyte. Carbon 72:381–386
55. Verma ML, Minakshi M, Singh NK (2014) Synthesis and Characterization of Solid Polymer Electrolyte based on Activated Carbon for Solid State Capacitor. Electrochim Acta 137:497–503
56. Minakshi M, Singh P, Sharma N, Backford M, Ionescu M (2011) Lithium Extraction-Insertion from/into LiCoPO4 in Aqueous Batteries. Ind Eng Chem Res 50:1899–1905
57. Verma ML, Minakshi M, Singh NK (2014) Structural and Electrochemical Properties of Nanocomposite Polymer Electrolyte for Electrochemical Devices. Ind Eng Chem Res 53: 14993–15001